tvst

DOI: 10.1167/tvst.6.5.12

Article

Characterization of Long Working Distance Optical Coherence Tomography for Imaging of Pediatric Retinal Pathology

Ruobing Qian[1], Oscar M. Carrasco-Zevallos[1], Shwetha Mangalesh[2], Neeru Sarin[2], Lejla Vajzovic[2], Sina Farsiu[1,2], Joseph A. Izatt[1,2], and Cynthia A. Toth[1,2]

[1] Department of Biomedical Engineering, Duke University, Durham, NC, USA
[2] Department of Ophthalmology, Duke University Medical Center, Durham, NC, USA

Correspondence: Cynthia A. Toth, Box 3802, Duke Eye Center, Durham, NC 27710, USA. e-mail: cynthia.toth@duke.edu

Received: 26 May 2017
Accepted: 28 August 2017
Published: 16 October 2017

Keywords: optical coherence tomography; retinal imaging; pediatric imaging; long working distance

Citation: Qian R, Carrasco-Zevallos OM, Mangalesh S, Sarin N, Vajzovic L, Farsiu S, Izatt JA, Toth CA. Characterization of long working distance optical coherence tomography for imaging of pediatric retinal pathology. Trans Vis Sci Tech. 2017;6(5):12, doi:10.1167/tvst.6.5.12

Purpose: We determined the feasibility of fovea and optic nerve head imaging with a long working distance (LWD) swept source optical coherence tomography (OCT) prototype in adults, teenagers, and young children.

Methods: A prototype swept source OCT system with a LWD (defined as distance from the last optical element of the imaging system to the eye) of 350 mm with custom fixation targets was developed to facilitate imaging of children. Imaging was performed in 49 participants from three age groups: 26 adults, 16 children 13 to 18 years old (teenagers), and seven children under 6 years old (young children) under an approved institutional review board protocol. The imaging goal was to acquire high quality scans of the fovea and optic nerve in each eye in the shortest time possible. OCT B-scans and volumes of the fovea and optic nerve head of each eligible eye were captured and graded based on four categories (lateral and axial centration, contrast, and resolution) and on ability to determine presence or absence of pathology.

Results: LWD-OCT imaging was successful in 88 of 94 eligible eyes, including seven of 10 eyes of young children. Of the successfully acquired OCT images, 83% of B-scan and volumetric images, including 86% from young children, were graded as high-quality scans. Pathology was observed in high-quality OCT images.

Conclusions: The prototype LWD-OCT system achieved high quality retinal imaging of adults, teenagers, and some young children with and without pathology with reasonable alignment time.

Translational Relevance: The LWD-OCT system can facilitate imaging in children.

Introduction

An estimated 19 million children worldwide are visually impaired, and 1.4 million are irreversibly blind.[1] To decrease the risk of blindness, it is critical to diagnose these children early and treat the evolving disease before permanent damage. Optical coherence tomography (OCT) is a diagnostic imaging modality that provides high resolution cross-sectional images of the human retina in vivo[2] and has become a standard clinical diagnostic tool for management of vitreoretinal diseases in adults and older children.[3,4] Clinical tabletop OCT systems have working distances of approximately 25 mm and require a chinrest to immobilize the patient. To acquire high-quality OCT images, these systems necessitate upright and cooperative patients who can fixate for seconds at a time with large instrumentation close to their face. Imaging in young children and toddlers, who are uncooperative and inherently afraid of objects close to their face, with conventional OCT is challenging. Thus, diagnostic retinal screening of this population currently is limited. The A-line rates of spectral-domain OCT clinical-grade systems also are limited to 20 to 68 kHz[5] and require several seconds for volumetric acquisition, which may be insufficient for imaging in young children who cannot adequately fixate for seconds at a time.

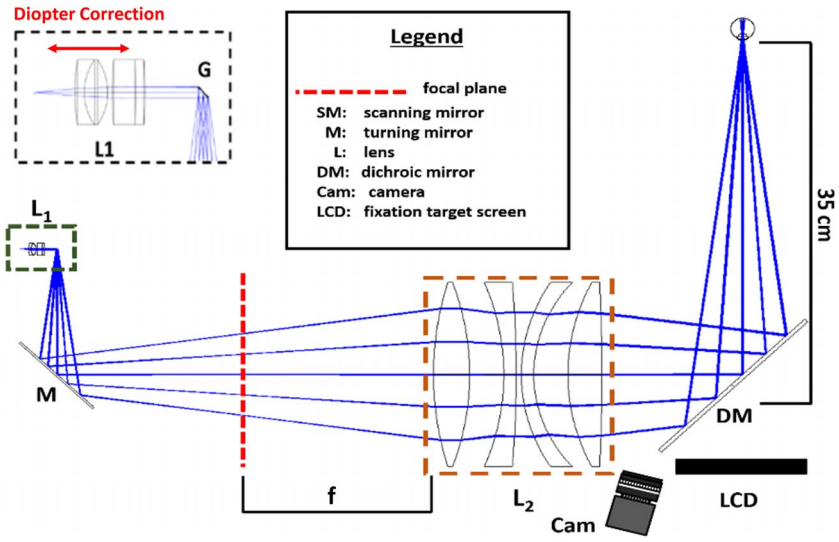

Figure 1. LWD OCT prototype sample arm. The distance between the dichroic mirror and the participant's eye is approximately 35 cm.

An alternative approach is to use handheld OCT (HHOCT) probes to image eyes in infants and young children in the supine position, either under sedation with general anesthesia[6–10] or without sedation.[11–13] Retinal imaging with HHOCT has contributed significantly to the understanding of the development of infant retina in vivo[14–20] and aided in uncovering microanatomic structural retinal changes in infants and children with retinopathy of prematurity,[11,15,17,21–26] albinism,[10] nystagmus,[27,28] and shaken baby syndrome.[7,29] However, similar to clinical OCT scanners, the HHOCT probe also must be placed approximately 25 mm away from the eye to achieve alignment and requires the child to be stable (and usually supine). While experts may be able to perform imaging in young children and infants sitting on a parent's lap or in the supine position while cradled in the parent's arms,[30] imaging in uncooperative young children and infants without sedation generally is difficult with current HHOCT systems.

To address the aforementioned challenges in pediatric OCT imaging, we developed a custom swept-source OCT system for fast volumetric imaging at a 100 kHz A-scan rate coupled to a novel OCT sample arm with a working distance of 350 mm and a field view of 16°.[31] We demonstrated that, using this long working distance OCT (LWD-OCT) system, we could acquire high-quality volumetric OCT scans with a 16° field of view in a few adults and one 6-year-old healthy child.[31] Here, we report on the results of a clinical study testing our LWD-OCT prototype to image healthy and diseased eyes of participants in three age groups: adults, teenagers, and young children. From this, we outlined an approach for pediatric imaging with LWD-OCT.

Methods

Prototype Design

The sample arm optical design of the prototype LWD-OCT (Fig. 1) was detailed by Carrasco-Zevallos et al.[31] The LWD-OCT used a 2f retinal scanning configuration with two custom lenses, L_1 and L_2, to reduce the number of optical elements and footprint of the system compared to traditional OCT systems using a 4f telescope. The working distance of the system (from the dichroic mirror to the participant's pupil) was 350 mm with a maximum scanning angle of 16°, limited by the diameter of L_2, with a lateral resolution of <10 μm over the entire angular scan range. The system had a refractive error correction range of −8 to +5 diopters. A liquid crystal display (LCD) screen (Lilliput Electronics, Inc., City of Industry, CA) was coaligned with the OCT system using a custom dichroic mirror (DM; OPCO Laboratory, Inc., Fitchburg, MA) and displayed a cross-hair target to facilitate fixation during imaging of adults and older children. During imaging of young children, the LCD screen displayed animation videos selected before the imaging session by each child based on his or her preference. Additionally, a pupil camera (Point Grey Research, Inc., Richmond, Canada) was used to facilitate initial lateral and axial alignment of the ocular pupil to the OCT beam. A

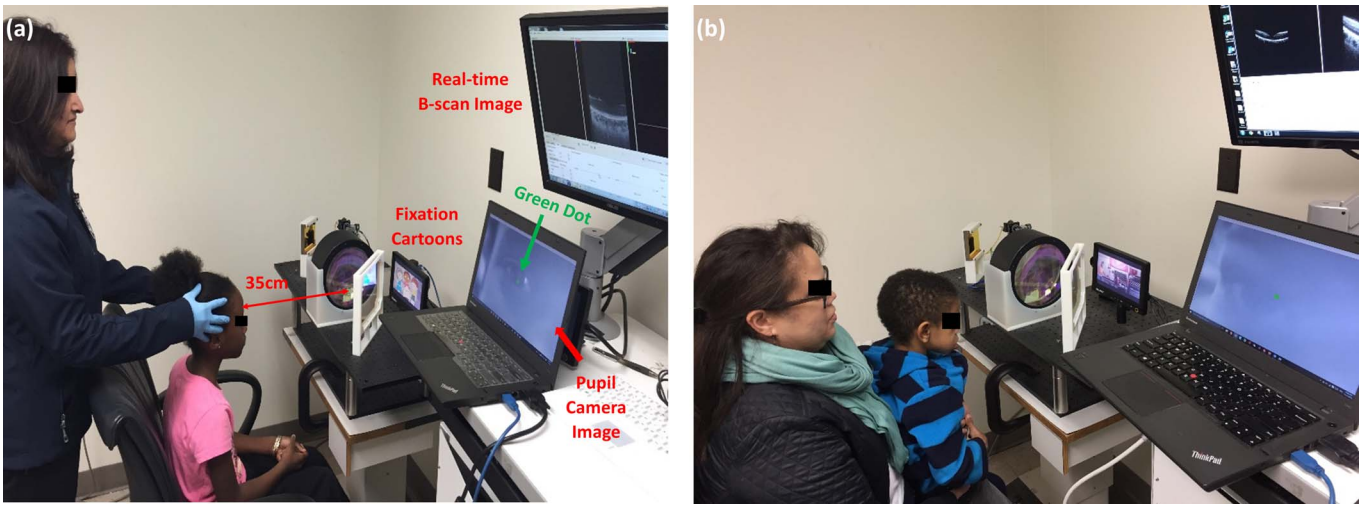

Figure 2. Demonstrations of the typical positioning of older and younger children with the imaging system. (a) A 9-year-old child aligned with the system by the operator. (b) A 2-year-old child seated in the parent's lap and aligned by the parent. (All photographs with parental permission.) The *green dot* on the pupil camera image indicates the location of the OCT beam.

green marker overlaid on the live pupil camera frames denoted the lateral position of the OCT beam.

The swept source OCT engine used a 1040 nm, 100 kHz swept laser source with an axial resolution of 8.12 μm, and the custom graphic processing unit (GPU) accelerated custom software enabled real-time volumetric imaging at 100k A-scans/second.[31]

Human Imaging

This prospective study was approved by the Duke University Medical Center Institutional Review Board, and it adhered to the Health Insurance Portability and Accountability Act and all tenets of the Declaration of Helsinki. Healthy volunteers and patients, adults and children, were enrolled after obtaining written informed consent from either the participant or from the legal guardian of the participant after explanation of the potential risks of the study. Eligible eyes for this pilot study could be healthy or exhibit pathology, and all eligible eyes were required to have media adequate for imaging and reasonable visual function (eyes with dense amblyopia or no light perception [NLP] vision were excluded). The optical power incident on the cornea at 1040 nm was measured at below 1.7 mW before and after all imaging sessions, which was well under the maximum permissible exposure determined by American National Standards Institute (ANSI) safety standards.

Images centered on the fovea and optic nerve head were attempted in each eye using the following protocol: B-scans comprised of 800 A-scans/B-scan and volumetric scans comprised of 800 A-scans/B-scan and 96 B-scans/volume. Radial scans with 800 A-scans/B-scan and 24 B-scans also were attempted in the adults and teenagers, but not in the young children due to the restricted imaging session time. The B-scan, volume, and radial scan frame rates were 125, 1.3, and 5.2 Hz, respectively.

The prospective study consisted of four sequential stages. In stage 1, the prototype LWD-OCT system was used to obtain images in 10 adults, with or without retinal pathology, to optimize the system design and imaging protocol. In stage 2, LWD-OCT imaging was obtained in 16 adults (8 with and 8 without pathology). In stage 3, LWD-OCT imaging was obtained in 16 children aged 13 to 18 years (called teenagers; 8 with and 8 without pathology). In the last stage, to test the feasibility of imaging in young children without a need for sedation and supine positioning, LWD-OCT imaging was obtained in children under 6 years old (called young children). To proceed from one stage to the next, a minimum of 80% of the scans for each scan type had to be graded as "good." The grading protocol is detailed in the Data Analysis section.

Alignment Protocol

Adults in the study (stages 1 and 2) were aligned laterally and axially using a chinrest mounted on a slit-lamp base. The green dot overlaid on the pupil camera images displayed on a computer monitor denoted the lateral position of the OCT beam to facilitate lateral alignment (Fig. 2a). For initial axial

alignment, the participant's head was translated until the pupil was in focus on the displayed pupil camera images. The final alignment was performed based on the real-time OCT images displayed on the custom software.

The final goal of the study was to align and perform imaging in young children without a chinrest, since children are inherently afraid of objects, including chinrests and slit-lamps, close to their face. In stage 3 of this study, the teenagers underwent imaging without a chinrest and the participant's head was held gently by the operator to align the system (Fig. 2a). The OCT system also was placed on a motorized table with an adjustable height to help facilitate vertical alignment. In stage 4 of the study, children aged 4 to 6 years were aligned using a method similar to that used for teenagers. Children under 4 years of age sat on the parent's lap during alignment (Fig. 2b). With guidance from the OCT operator, the parent then adjusted the child's body and head position to align the system based on the pupil camera image feedback. The LCD screen displayed fixation cartoons to attract the child's attention.

Survey

A survey study was conducted with the participant after the imaging session. For the young child under 4 years old, the survey was conducted with the participant's legal guardian. The survey consists of four questions: (1) Was the imaging session too long? (Yes/No for the first 10 adults, and too long/acceptable/excellent for the rest of the participants), (2) Was the fixation difficult? (Yes/No for the first 10 adults, and hard/okay/easy for the rest of the participants), (3) Was it difficult to hold steady for imaging? (Not included in the survey of first 10 adults, hard/okay/easy for the rest of the participants), and (4) Was the imaging session uncomfortable? (Yes/No for the first 10 participants, and uncomfortable/okay/comfortable for the rest of the participants)

Volume Motion Artifact Correction

Despite improvement in the imaging acquisition speed with the swept source OCT system, artifacts due to the participant's motion still were present in the volumetric images and degraded the quality of the acquired volumes. Additionally, motion artifacts were more noticeable when aligning the participant without a chinrest (stages 3 and 4) compared to when using a chin rest (stages 1 and 2), which is the convention method of alignment for the clinical OCT system. Without a chin rest, axial motion was more noticeable since the child's head was stabilized gently laterally (by the imager or parent) without forehead support. Motion artifacts in acquired volume were corrected in postprocessing using the following correction algorithm specifically written in MATLAB (Mathworks, Natick, MA) for this study: (1) Lateral and axial motion between subsequent B-scans was estimated from the peak of the cross-correlation between them, and all B-scans were registered to the first one used as a key frame. (2) The top of the inner segment/outer segment (IS/OS) junction layer in the central B-scan of the fovea in the volumetric image was segmented[32] to obtain an estimate of retinal curvature. (3) To recover the approximate retinal curvature in the slow scan direction, all B-scans were shifted axially to match the estimated retinal curvature in the slow scanning axis.

The motion artifact algorithm is illustrated in Figure 3 with representative volumetric foveal images of a 6-year-old child. All OCT volumes acquired in the study with significant axial motion artifacts were corrected using the algorithm described above. The motion artifacts in the volume of the optic nerve head also were corrected in postprocessing using step 1 of the above algorithm.

Data Analysis

The B-scans and OCT volumes of the first 10 adults acquired were graded by two independent graders (SM, LV) based on four categories: lateral and axial centration of the fovea or optic nerve head, contrast, and resolution. A scoring system was devised and each category was given a mark: 2 for high quality, 1 for acceptable, or 0 for unacceptable scans. Analysis of results showed that there was 100% intergrader agreement on scoring of each type of scans of all 10 adults; therefore, the rest of the images were graded by a single grader (SM) based on this scoring system. The total score was defined as a sum of all categorical marks and the highest attainable score was 8. The scan was deemed high quality if the total score was 7 or 8 and acceptable if the score was 5 or greater. For the overall quality of the volumetric image, the grade was given for the best single B-scan in the volume. Further, the best foveal scan acquired from each eye was chosen to assess the presence of retinal layers and pathology at the fovea. Similarly, for the optic nerve scans, the overall volume, as well as the ability to capture the entire optic nerve was assessed.

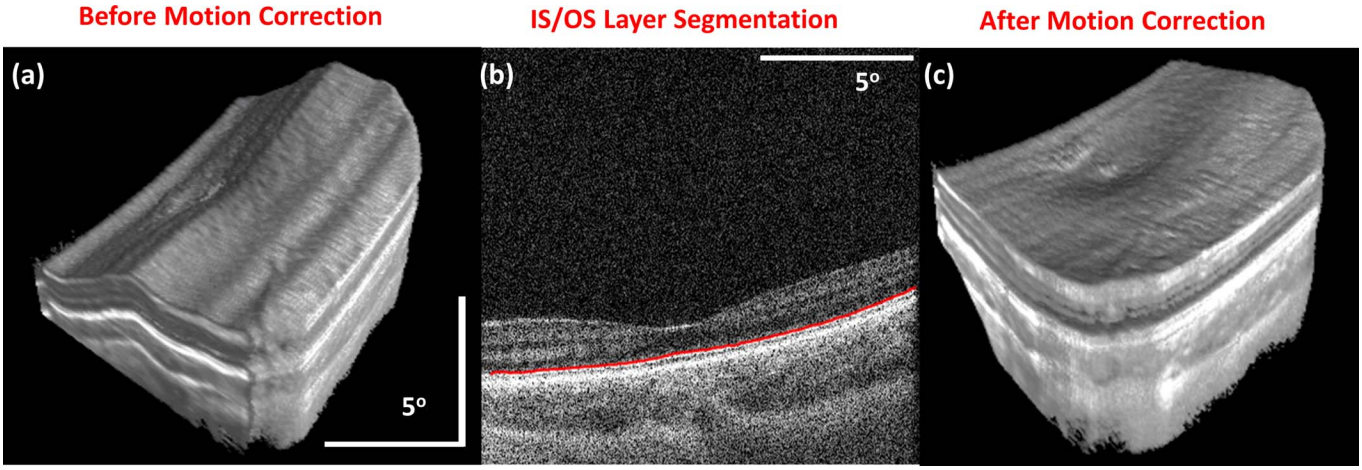

Figure 3. (a) Volumetric image centered on the fovea of a 6-year-old child before motion correction. (b) Single B-scan at the center of the fovea with a segmentation line (*red*) at the top of the IS/OS band. (c) The same volumetric image after motion correction.

To address a primary outcome of whether successful imaging was possible with this system, we recorded the percentage of eligible eyes that were imaged successfully with LWD-OCT. To address the second primary outcome of whether high-quality images of the fovea and optic nerve head could be acquired with LWD-OCT, the average score of each imaged eye was calculated by averaging the scores of three categories of images: B-scans of fovea, volumes of fovea and optic nerve head. The radial scans of the fovea were not included in calculating the average scores, since they were acquired only in the adults and teenagers. To address a secondary outcome of whether the quality of captured images was comparable across age groups, the Wilcoxon signed-rank test was used to compare the average grading scores for pairs of age groups (adults vs. teenagers vs. young children) to assess whether image quality of the LWD-OCT prototype system is consistent among all age groups. The null hypothesis was that image quality scores were not significantly different among all age groups, and a P value lower than 0.05 was deemed statistically significant.

The alignment time was another key parameter used to assess the performance of the prototype system, especially in pediatric imaging. The alignment start time was defined as the time point when the imager first obtained rough alignment of the participant's pupil within the field of view of the pupil camera, and commenced acquisition of B-scan images. The alignment stop time was defined as clear and constant visualization of the fovea in the real-time B-scan images.

Results

We enrolled 26 adults (10 with and 16 without pathology), 16 teenagers (eight with and eight without pathology), and seven young children (four with and three without pathology) in this prospective study. The total number of participants, eyes, and eyes with acquired images in each age group are shown in Table 1. In four of the young children (21 months, and 2, 2, and 3 years old), one eye of each participant was excluded from the study due to unmeasurable low vision with amblyopia, retinoschisis detachment with scarring, no light perception with massive coloboma, or parents' decisions not to proceed with research imaging.

Table 1. Number of Enrolled Participants, Eligible Eyes, and Eyes That Were Successfully Imaged

Age Group, y	Total Number of Participants	Total Number of Eligible Eyes	Total Number of Eyes with Acquired Images *N* (%)
Adults	26	52	50 (96.2)
Teenagers, 13–18 y	16	32	31 (96.9)
Young children, 13 mos–6 y	7	10	7 (70)
Total	49	94	88 (95.7)

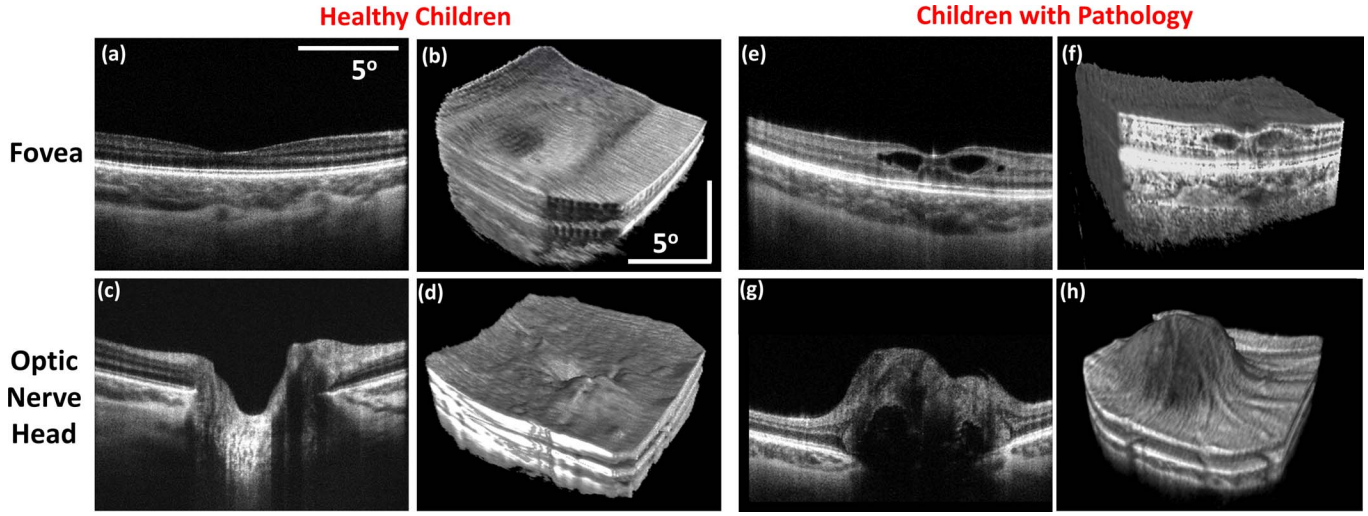

Figure 4. Representative SSOCT images acquired from a teenager and young child with and without pathology are illustrated and obtained with the prototype system. (a) Ten averaged B-scans of a healthy 6-year-old child. (b) Volume of the fovea of a healthy 2-year-old child. (c, d) Ten averaged B-scans and volume of optic nerve of a healthy 6-year-old child. (e, f) Ten averaged B-scans and the cross section of volume of a 5-year-old child with retinoschisis. (g, h) Ten averaged B-scans and volume of a 16-year-old child with optic nerve head elevation. All B-scans and volumetric images here were graded as high-quality scans.

Of all of the study eligible eyes, 50 of 52 adult eyes (96.2%) and 29 of 30 teenager eyes (96.9%) were successfully imaged. Among the adults, two eyes from one participant were not imaged successfully due to a temporary system malfunction. Among the teenagers, one eye was not imaged successfully because the participant had very high diopter (+23 D) customized contact lens. Among the young children with eligible eyes, three eyes from two children (13 months and 2 years old) were not imaged successfully because they were uncooperative and unable to maintain fixation. The youngest child with successful imaging was 21 months old.

Young Children Imaging

Representative B-scans and volumes of the fovea and optic nerve head of normal participants in the children younger than age six are shown in Figures 4a to 4d. Retinal pathology, such as optic nerve head elevation, outer plexiform layer (OPL) disruption, retinoschisis, and subretinal fluid also were identified successfully in the pediatric group using the prototype system. Some representative B-scans and volumetric images with pathology are shown in Figures 4e to 4h.

Imaging Grading

Among all the successful imaging sessions, the overall percentages of images with grading scores higher than or equal to 7 (good scans) in each age group were 82%, 84%, and 86% (Table 2). The average score for the adults ($n = 50$) was 7.29 ± 1.01. The average score for teenagers ($n = 31$) was 7.24 ± 1.39, and the average grade for young children ($n = 7$) was 7.31 ± 1.00, and image quality in the different

Table 2. Results of Grading of SSOCT Images for Each Age Group

Age Group (Number of Eyes with Scans)	Acceptable Scans Percentage (% with Score ≥ 5)					High Quality Scans Percentage (% with Score ≥ 7)				
	Foveal B-Scans	Foveal Volume	Foveal Radial Scans	Optic Nerve	Overall	Foveal B-Scans	Foveal Volume	Foveal Radial Scans	Optic Nerve	Overall
Adults ($n = 50$)	98%	96%	96%	100%	98%	82%	86%	82%	93%	82%
Teenagers ($n = 31$)	100%	97%	100%	93%	97%	90%	80%	85%	87%	84%
Young Children ($n = 7$)	100%	83%	–	100%	100%	86%	83%	–	100%	86%
Total ($n = 88$)	99%	96%	97%	97%	97%	85%	84%	83%	91%	83%

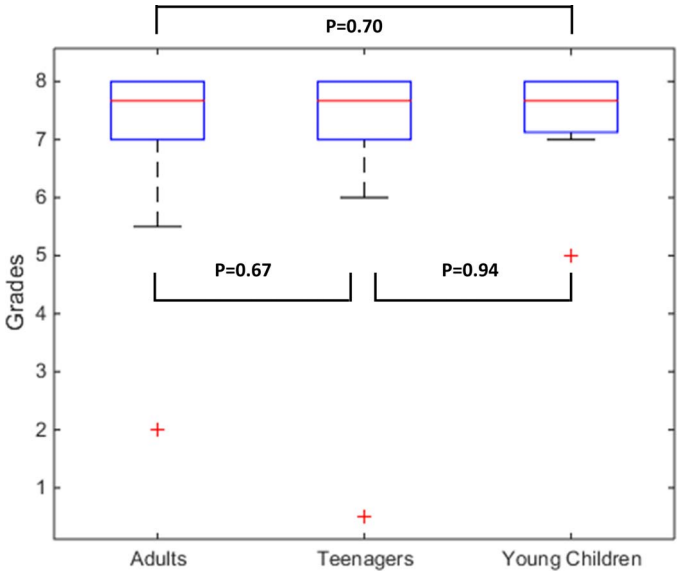

Figure 5. Boxplot of image grading scores of three age groups in the study, and results of the Wilcoxon rank sum test between every pair of two age groups. Outliers are defined as the scores larger than 1.5 times the interquartile range of the box.

age groups did not demonstrate significant differences by the 2-sided Wilcoxon rank sum test (Fig. 5). Note that the two enrolled eyes of adults and the three enrolled eyes of young children that were not imaged successfully were excluded from statistical analysis of grading.

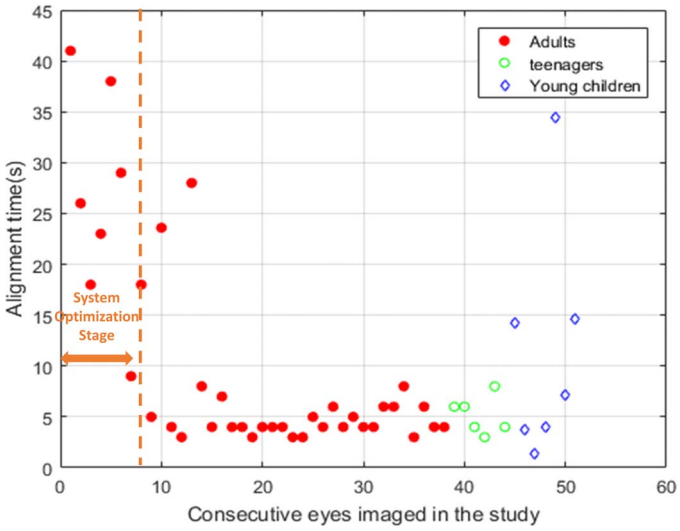

Figure 6. Alignment time of 38 eyes of adults (*red dots*), six eyes of teenagers (*green circles*), and seven eyes of young children (*blue diamonds*).

System Alignment

An important parameter to evaluate the difficulty of alignment is alignment time (defined in the Methods section). The alignment time of 38 eyes of adults, six eyes of teenagers, and seven eyes of young children were measured (Fig. 6). It should be noted that the alignment time of the first eight eyes in the study was relatively longer, because the green dot marker in the pupil camera image indicating the OCT beam location was not fully calibrated. Additionally, the examiner was not experienced in operating the system in the initial part of the study. As a result, the alignment times of the first eight eyes were excluded from the statistical analysis below.

The average alignment time across all three age groups ($n = 43$) was 6.8 $\pm$ 6.7 seconds. The average alignment times in adults (red dots in Fig. 6, $n = 30$), teenagers (green circles in Fig. 6, $n = 6$), and young children (blue diamonds in Fig. 6, $n = 7$) were 6.0 $\pm$ 5.6, 5.2 $\pm$ 1.8, and 11.4 $\pm$ 11.4 seconds. It should be noticed that the average alignment time in young children was calculated based on 7 of 10 eyes that were imaged successfully.

Survey Outcomes

All 49 participants were enrolled in the survey. A total of 46 of the 49 (94%) participants, including all seven young children (100%), indicated that the imaging time was not too long. All three participants who considered the imaging time too long were those enrolled during the optimization stage of the study. A total of 47 of 49 (96%) participants, including five of seven young children (71%), did not feel that fixation was difficult to achieve and maintain. Two young children, whose parents considered the fixation difficult, were participants from whom OCT images were not acquired successfully. A total of 35 of 39 (90%) participants, including five of seven young children, did not believe that holding steady during the imaging session was too hard. It should be noted that this question was not included in the survey of first 10 adults, which resulted in the total number of participant feedback responses to this question being 39 instead of 49. Of all 18 participants who underwent imaging while the imager gently held the participants' head (Fig. 2a), 15 (83%) considered it easy or okay to hold steady, while the parents of four of five (80%) children younger than 4 years old who were situated in the parents' laps (Fig. 2b) considered it easy or OK to hold steady. A total of 46 of 49 (94%) participants, including all seven young chil-

Table 3. The Survey Results of Each Age Group in This Study

	First 10 Adults *N* (%)	The Rest Adults *N* (%)	Teenagers *N* (%)	Young Children *N* (%)	Total* *N* (%)
Was imaging session too long?					
Yes	2 (20%)	1 (6%)	0 (0%)	0 (0%)	3 (6%)
Acceptable	8 (80%)	12 (75%)	13 (81%)	6 (86%)	46 (94%)
Excellent		3 (19%)	3 (19%)	1 (14%)	
Was the fixation difficult?					
Hard	0 (0%)	0 (0%)	0 (0%)	2 (29%)	2 (4%)
Okay	10 (100%)	2 (13%)	5 (31%)	2 (29%)	47 (96%)
Easy		14 (87%)	11 (69%)	3 (43%)	
Was it difficult to hold steady for imaging?					
Hard		1 (6%)	1 (6%)	2 (29%)	4 (10%)
OK	N/A	4 (25%)	6 (38%)	4 (57%)	14 (36%)
Easy		11 (69%)	9 (56%)	1 (14%)	21 (54%)
Was the imaging session comfortable?					
Uncomfortable	2 (20%)	1 (6%)	0 (0%)	0 (0%)	3 (6%)
Okay	8 (80%)	3 (19%)	6 (37%)	3 (43%)	46 (94%)
Comfortable		12 (75%)	10 (63%)	4 (57%)	

* To combine the survey results of the first 10 adults with the rest of the participants in this column, we collapsed acceptable/excellent imaging session time (Question 1), okay and easy fixation (Question 2), and comfortable and okay imaging session (Question 4).

dren, thought the overall imaging session was OK or comfortable.

Discussion

In this study, we demonstrated the use of a prototype LWD-OCT system with a working distance of 350 mm to image eyes in young children under 6 years old without sedation and a chinrest and with a reasonable alignment time. OCT systems with long working distances have been developed previously for endoscopic imaging probes (up to 80 mm)[33] for tissue imaging and microscope-integrated OCT systems (up to 175 mm)[34–36] for intraoperative imaging. To our knowledge, this is the longest working distance OCT system that has been reported. The 2f optical relay, which has been implemented previously in scanning laser ophthalmoscopes (SLO)[37,38] and adaptive optics SLO,[39] greatly reduced the footprint and weight of the system. The system also used a 100 KHz swept source, which has a faster A-scan rate than most commercial spectral domain OCT systems, and it allows volumetric imaging of the retina in as shorter imaging time with less motion artifacts.

The current study was conducted in three age groups: adults, teenagers, and young children. In young children, we were able to image only seven of 10 eyes with this system. It is important to note that in one of these children aged 21 months old, however, no clinical OCT imaging was possible due to the participant's inability to fixate in front of the tabletop system, yet we were able to image the macula with the LWD OCT system.

For eyes in which OCT images were acquired successfully, there was no significant difference in image quality grades between the age groups with 5% significance levels, and the overall percentages of high quality scans were higher than 80% for each age group. While cooperation still was a challenge in two young children (three eyes) when using the current tabletop setup, when images could be captured, they generally were very high quality volume and B-scan images of the macula and optic nerve head. The mean alignment time was 11.4 seconds for young children when OCT images were captured successfully, indicating the feasibility of alignment of young children and infants without use of a chinrest and the supine position using LWD-OCT.

Handheld OCT probes have shown great promise in young children and for infant bedside imaging. However, handheld OCT imaging in young children

and infants without use of sedation and the supine position generally is difficult. In contrast, with our LWD-OCT system we have the ability to image eyes in young children while they were comfortable and with minimal restraint sitting on their parent's laps and watching cartoons on the LCD screen in front of them. In addition, our LWD-OCT system allowed participants to maintain a comfortable distance from the "intimidating" instrument.

One of the major limitations of our LWD-OCT system is the absence of an automatic tracking and alignment system, and it was the main reason why we did not successfully image three eyes of young children in the study. The current system alignment relies on the participant's parents or examiners gently holding and adjusting the position of the participants' head as well as the operator adjusting the height of the instrument table based on the feedback from the pupil camera and the real-time OCT images. These requirements to acquire high quality images in children may increase alignment difficulty and introduce more motion artifacts. Future work may include placing the OCT sample arm on a three-dimensional motorized translational stage, using additional methods to detect fixation,[40] and implementing the pupil tracking technology into the current prototype system,[41] so that the system can be aligned with the participant automatically based on the pupil position extracted from the pupil tracking system, and the alignment time potentially could be reduced. An automatic tracking and alignment system potentially can facilitate LWD-OCT imaging of young uncooperative children.

In the study, we also noticed that our current fixation targets and cartoon movies sometimes did not attract the child's attention, especially when imaging eyes in children younger than 3 years. Moreover, the visible prototype optical elements, such as the large objective lens, distracted the child from the fixation movies. In the future, more age-specific fixation targets or cartoon movies will be used.[42] Additionally, all optical elements of the system will be housed in an enclosure to ensure the participant does not become distracted.

Another limitation is the motion artifacts in volumetric images. The motion artifacts were inevitable as the participants underwent imaging without a chinrest and were positioned further away from the system compared to the conventional tabletop OCT systems. We applied a motion artifact correction algorithm to correct axial and lateral motion along the B-scan direction in the volume as shown above (Fig. 3). Although the algorithm partially compensated for participant motion during image acquisition to generate high quality image volumes, it made several assumptions (such as that the retinal curvature in fast and slow OCT acquisition directions was the same) that should limit extraction of quantitative morphologic data from the acquired image volumes. Additionally, other motion artifacts, such as lateral and rotational motion out of the B-scan plane, could not be corrected using the current setting, which may affect the visualization of volumes. A more robust method to remove motion artifacts in volumes is to use an orthogonal scan pattern,[43,44] which will be considered in future studies.

Another potential improvement would be to use an OCT light source with much longer instantaneous coherence length, such as a vertical cavity surface-emitting laser (VCSEL), which has a theoretical imaging range of more than one meter,[45] compared to 7.4 mm in our current prototype system. In general, the axial alignment of the LWD-OCT system is more difficult than with a conventional tabletop OCT system, since the participant's eye is much further away from the system and not fixed by the chinrest. A much longer imaging range potentially could help the imager locate the participant's axial position much easily; however, such light sources and the related acquisition systems are not yet clinically viable.

In summary, we successfully captured high quality retinal images of adults, teenagers, and young children with and without pathology using our prototype LWD-OCT system. Furthermore, we successfully imaged eyes in children as young as 21 months old without sedation in the clinic. Additional studies, such as comparative studies among the LWD, conventional tabletop, and handheld probe OCT system, are needed to further validate the use of our prototype.

Supplement

All images in Figure 7 had relatively worse image contrast and resolution compared to the high-quality images in Figure 4. Figure 7a had relatively worse image resolution possibly due to imperfect diopter correction or dispersion compensation. Moreover, the fovea scan in Figure 7a was not accurately centered vertically, as parts of the choroid were out of the imaging range. Figure 7b had relatively worse image resolution and contrast possibly due to high astigma-

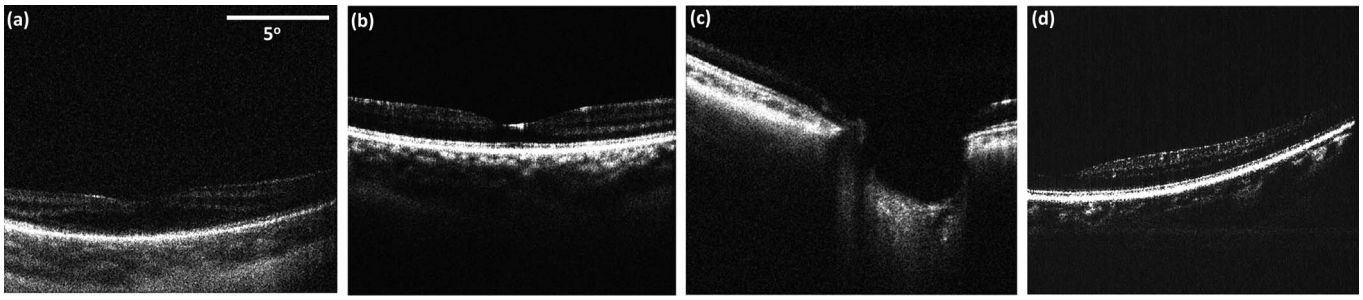

Figure 7. Representative "acceptable" (score between 5 and 6) and "unacceptable" (score under 5) quality images from participants with and without pathology are illustrated and obtained with the prototype system. (a) Seven averaged B-scans of fovea of a 21-month-old child with possible cysts or split in the inner nuclear layer. The total score is 5 (contrast, 1; resolution, 1; lateral centration, 2; vertical centration, 1). (b) Ten averaged B-scans of fovea of a 16-year-old teenager with +4.25 D astigmatism. The total score is 6 (contrast, 1; resolution, 1; lateral centration, 2; vertical centration, 2). (c) Ten averaged B-scans of optic nerve of a 17-year-old teenager with congenital glaucoma (severe stage) with eccentric fixation. The total score is 6 (contrast, 1; resolution, 1; lateral centration, 2; vertical centration, 2). (d) Ten averaged B-scans of fovea of a 51-year-old adult. The total score is 4 (contrast, 1; resolution, 1; lateral centration, 0; vertical centration, 2).

tism. The fovea scan in Figure 7d was graded as "unacceptable," as the fovea was off-centered.

Acknowledgments

The authors thank Niklas Gahm and Gar Waterman for assistance in optomechanical design, Brenton Keller for assistance in pupil camera setup, and Boris Gramatikov and David Guyton (Johns Hopkins University, Baltimore, MD) for fruitful discussions.

Supported by the Hartwell Foundation and National Institutes of Health Bioengineering Research Partnership Grant R01-EY023039.

Disclosure: **R. Qian**, None; **O.M. Carrasco-Zevallos**, None; **S. Mangalesh**, None; **N. Sarin**, None; **L. Vajzovic**, Alcon (I), Second Sight (I), F Hoffmann-La Roche Ltd (I); **S. Farsiu**, Duke (P); **J.A. Izatt**, Leica (P, I); **C.A. Toth**, Alcon (P), Genetech (F), Leica (F)

References

1. Organization WH. Visual impairment and blindness. Geneva: WHO; 2014.
2. Huang D, Swanson EA, Lin CP, et al. Optical Coherence Tomography. *Science*. 1991;254:1178–1181.
3. Mirza RG, Johnson MW, Jampol LM. Optical coherence tomography use in evaluation of the vitreoretinal interface: a review. *Surv Ophthalmol*. 2007;52:397–421.
4. Stopa M, Bower BA, Davies E, Izatt JA, Toth CA. Correlation of pathologic features in spectral domain optical coherence tomography with conventional retinal studies. *Retina-J Ret Vit Dis*. 2008;28:298–308.
5. Zhang Q, Lee CS, Chao J, et al. Wide-field optical coherence tomography based microangiography for retinal imaging. *Sci Rep*. 2016;6:22017.
6. Dayani PN, Maldonado R, Farsiu S, Toth CA. Intraoperative use of handheld spectral domain optical coherence tomography imaging in macular surgery. *Retina-J Ret Vit Dis*. 2009;29:1457–1468.
7. Scott AW, Farsiu S, Enyedi LB, Wallace DK, Toth CA. Imaging the infant retina with a hand-held spectral-domain optical coherence tomography device. *Am J Ophthalmol*. 2009;147:364–373.
8. Jung W, Kim J, Jeon M, Chaney EJ, Stewart CN, Boppart SA. Handheld optical coherence tomography scanner for primary care diagnostics. *IEEE T Bio-Med Eng*. 2011;58:741–744.
9. LaRocca F, Nankivil D, DuBose T, Toth CA, Farsiu S, Izatt JA. In vivo cellular-resolution retinal imaging in infants and children using an ultracompact handheld probe. *Nat Photon*. 2016;10:580–584.
10. Chong GT, Farsiu S, Freedman SF, et al. Abnormal foveal morphology in ocular albinism imaged with spectral-domain optical coherence tomography. *Arch Ophthalmol-Chic*. 2009;127:37–44.
11. Chavala SH, Farsiu S, Maldonado R, Wallace DK, Freedman SF, Toth CA. Insights into

advanced retinopathy of prematurity using handheld spectral domain optical coherence tomography imaging. *Ophthalmology*. 2009;116:2448–2456.
12. Patel A, Purohit R, Lee H, et al. Optic nerve head development in healthy infants and children using handheld spectral-domain optical coherence tomography. *Ophthalmology* 2016;123:2147–2157.
13. Maldonado RS, Izatt JA, Sarin N, et al. Optimizing hand-held spectral domain optical coherence tomography imaging for neonates, infants, and children. *Invest Ophthalmol Vis Sci*. 2010;51:2678–2685.
14. Vajzovic L, Hendrickson AE, O'Connell RV, et al. Maturation of the human fovea: correlation of spectral-domain optical coherence tomography findings with histology. *Am J Ophthalmol*. 2012; 154:779–789.
15. Maldonado RS, O'Connell RV, Sarin N, et al. Dynamics of human foveal development after premature birth. *Ophthalmology*. 2011;118:2315–2325.
16. Lee H, Proudlock F, Gottlob I. Is handheld optical coherence tomography reliable in infants and young children with and without nystagmus? Reliability of handheld OCT in young children. *Invest Ophthalmol Vis Sci*. 2013;54:8152–8159.
17. Vajzovic L, Rothman AL, Tran-Viet D, Cabrera MT, Freedman SF, Toth CA. Delay in Retinal Photoreceptor Development In Very Preterm Compared To Term Infants. *Invest Ophthalmol Vis Sci*. 2015;56:908–913.
18. Vinekar A, Avadhani K, Sivakumar M, et al. Understanding clinically undetected macular changes in early retinopathy of prematurity on spectral domain optical coherence tomography. *Invest Ophthalmol Vis Sci*. 2011;52:5183–5188.
19. Vinekar A, Mangalesh S, Jayadev C, Maldonado RS, Bauer N, Toth CA. Retinal imaging of infants on spectral domain optical coherence tomography. *Biomed Res Int*. 2015; 2015;782420.
20. Mallipatna A, Vinekar A, Jayadev C, et al. The use of handheld spectral domain optical coherence tomography in pediatric ophthalmology practice: our experience of 975 infants and children. *Indian J Ophthalmol*. 2015;63:586–593.
21. Maldonado RS, Yuan E, Tran-Viet D, et al. Three-dimensional assessment of vascular and perivascular characteristics in subjects with retinopathy of prematurity. *Ophthalmology*. 2014; 121:1289–1296.
22. Maldonado RS, Toth CA. Optical coherence tomography in retinopathy of prematurity looking beyond the vessels. *Clin Perinatol*. 2013;40: 271–296.
23. Rothman AL, Du TV, Vajzovic L, et al. Functional outcomes of young infants with and without macular edema. *Retina-J Ret Vit Dis*. 2015;35:2018–2027.
24. Erol MK, Ozdemir O, Coban DT, et al. Macular findings obtained by spectral domain optical coherence tomography in retinopathy of prematurity. *J Ophthalmol*. 2014;2014:468653.
25. Vinekar A, Mangalesh S, Jayadev C, et al. Macular edema in Asian Indian premature infants with retinopathy of prematurity: Impact on visual acuity and refractive status after 1-year. *Indian J Ophthalmol*. 2015;63:432–437.
26. Dubis AM, Subramaniam CD, Godara P, Carroll J, Costakos DM. Subclinical macular findings in infants screened for retinopathy of prematurity with spectral-domain optical coherence tomography. *Ophthalmology*. 2013;120:1665–1671.
27. Cronin TH, Hertle RW, Ishikawa H, Schuman JS. Spectral domain optical coherence tomography for detection of foveal morphology in patients with nystagmus. *J AAPOS*. 2009;13: 563–566.
28. Lee H, Sheth V, Bibi M, et al. Potential of handheld optical coherence tomography to determine cause of infantile nystagmus in children by using foveal morphology. *Ophthalmology*. 2013; 120:2714–2724.
29. Muni RH, Kohly RP, Sohn EH, Lee TC. Handheld spectral domain optical coherence tomography finding in shaken-baby syndrome. *Retina*. 2010;30:S45–50.
30. Lee H, Purohit R, Patel A, et al. In vivo foveal development using optical coherence tomography. *Invest Ophthalmol Vis Sci*. 2015;56:4537–4545.
31. Carrasco-Zevallos OM, Qian R, Gahm N, Migacz J, Toth CA, Izatt JA. Long working distance OCT with a compact 2f retinal scanning configuration for pediatric imaging. *Opt Lett*. 2016;41:4891–4894.
32. Chiu SJ, Li XT, Nicholas P, Toth CA, Izatt JA, Farsiu S. Automatic segmentation of seven retinal layers in SDOCT images congruent with expert manual segmentation. *Opt Express*. 2010; 18:19413–19428.
33. Guo SG, Hutchison R, Jackson RP, et al. Office-based optical coherence tomographic imaging of human vocal cords. *J Biomed Opt*. 2006;11:30501.
34. Boppart SA, Bouma BE, Pitris C, Southern JF, Brezinski ME, Fujimoto JG. Intraoperative assessment of microsurgery with three-dimension-

al optical coherence tomography. *Radiology*. 1998;208:81–86.
35. Carrasco-Zevallos OM, Keller B, Viehland C, et al. Live volumetric (4D) visualization and guidance of in vivo human ophthalmic surgery with intraoperative optical coherence tomography. *Sci Rep*. 2016;6:31689.
36. Tao YK, Srivastava SK, Ehlers JP. Microscope-integrated intraoperative OCT with electrically tunable focus and heads-up display for imaging of ophthalmic surgical maneuvers. *Biomed Opt Express*. 2014;5:1877–1885.
37. Sharp PF, Manivannan A. The scanning laser ophthalmoscope. *Phys Med Biol*. 1997;42:951–966.
38. Webb RH, Hughes GW, Delori FC. Confocal scanning laser ophthalmoscope. *Appl Optics*. 1987;26:1492–1499.
39. Dubra A, Gómez-Vieyra A, Díaz-Santana L, Sulai Y. Optical design of clinical adaptive optics instruments for retinal imaging. In: *Frontiers in Optics 2010/Laser Science XXVI*. Rochester, NY: Optical Society of America; 2010:FTuB3.
40. Irsch K, Gramatikov BI, Wu YK, Guyton DL. New pediatric vision screener employing polarization-modulated, retinal-birefringence-scanning-based strabismus detection and bull's eye focus detection with an improved target system: opto-mechanical design and operation. *J Biomed Opt*. 2014;19:067004.
41. Carrasco-Zevallos O, Nankivil D, Keller B, Viehland C, Lujan BJ, Izatt JA. Pupil tracking optical coherence tomography for precise control of pupil entry position. *Biomed Opt Express*. 2015;6:3405–3419.
42. Gramatikov BI, Rangarajan S, Irsch K, Guyton DL. Attention attraction in an ophthalmic diagnostic device using sound-modulated fixation targets. *Med Eng Phys*. 2016;38:818–821.
43. Kraus MF, Potsaid B, Mayer MA, et al. Motion correction in optical coherence tomography volumes on a per A-scan basis using orthogonal scan patterns. *Biomed Opt Express*. 2012;3:1182–1199.
44. Lezama J, Mukherjee D, McNabb RP, Sapiro G, Kuo AN, Farsiu S. Segmentation guided registration of wide field-of-view retinal optical coherence tomography volumes. *Biomed Opt Express*. 2016;7:4827–4846.
45. Wang Z, Potsaid B, Chen L, et al. Cubic meter volume optical coherence tomography. *Optica*. 2016;3:1496–1503.